coatings

MDPI

Article

Effect of Layer Number on Hydrogen Barrier Performance of Epoxy Composite Coatings

Hengpei Pan [1,2], Jiarui Deng [3], Heng Lv [4], Qianqian Chen [1], Pan Liu [1,2,*], Xiaoqin Zha [1,2] and Keren Zhang [3,*]

[1] Luoyang Ship Material Research Institute, Luoyang 471023, China; panhengpei@126.com (H.P.); chenqianqian0903@163.com (Q.C.); 201201@xsyu.edu (X.Z.)
[2] State Key Laboratory for Marine Corrosion and Protection, Luoyang 471023, China
[3] School of Materials Science and Engineering, Xi'an Shiyou University, Xi'an 710065, China; 18392705314@163.com
[4] Xi'an Special Equipment Inspection and Testing Institute, Xi'an 710054, China; 15229230668@163.com
* Correspondence: liupan_lp@163.com (P.L.); zkrnwpu@163.com (K.Z.)

Abstract

To improve the hydrogen barrier protection performance of pipeline steel used in hydrogen transmission pipelines, this study designs epoxy resin (EP) composite coatings of different structures, including pure epoxy coatings, epoxy/graphene bilayer coatings (EP/GC), and two types of EP/GC/EP three-layer sandwich structure coatings. The effects of the coating structure on hydrogen barrier performance, interfacial bonding strength, and corrosion resistance were systematically studied. The results show that the hydrogen barrier performance of the three-layer sandwich structure coating is significantly superior to that of the two-layer and pure epoxy coatings. Among them, the EP/GC/EP three-layer coating has the lowest effective hydrogen diffusion coefficient of 4.08×10^{-8} cm^2/s, about 95% lower than that of the X80 steel matrix, and the hydrogen permeability reduction coefficient (PRF) reaches 25.51. Adhesion tests showed that the double-layer coating had the highest bonding strength, reaching 19.6 MPa, while the three-layer coating decreased (10–11 MPa) due to increased interlayer interfaces. The electrochemical test results showed that the three-layer coating had the most positive self-corrosion potential (−0.37 V) and the lowest self-corrosion current density, demonstrating optimal corrosion resistance. The multilayer coating prepared in this study combines low cost, good adhesion, and excellent hydrogen resistance and corrosion resistance, providing an experimental and theoretical basis for the structural design of high-resistance hydrogen coatings on the inner walls of hydrogen transmission pipelines.

Keywords: graphene; epoxy resin; multilayer coating; hydrogen barrier performance; X80 pipeline steel; hydrogen penetration

Check for updates

Academic Editor: Tadeusz Hryniewicz

Received: 21 September 2026
Revised: 26 October 2026
Accepted: 28 October 2026
Published: 17 November 2026

Copyright: © 2026 by the authors. Licensee MDPI, Basel, Switzerland. This article is an open access article distributed under the terms and conditions of the Creative Commons Attribution (CC BY) license.

1. Introduction

As the global energy structure accelerates toward low-carbon transformation, hydrogen energy, as a widely sourced, high-calorific-value, and zero-carbon secondary clean energy source, plays an increasingly important role in achieving the goals of "carbon peaking and carbon neutrality" [1,2]. The hydrogen energy industry chain covers multiple stages, including production, storage, transportation, and end-use applications, with safe and efficient hydrogen transportation being the core hub connecting upstream production and downstream consumption. Among the many hydrogen delivery methods, pipeline transportation is regarded as the preferred solution for large-scale, long-distance hydrogen delivery in

the future due to its advantages of large volume, low costs, and strong continuity [3,4]. However, hydrogen pipelines have always faced a severe technical challenge during actual service: hydrogen embrittlement [5,6]. For hydrogen pipelines using high-strength pipeline steels such as X70 and X80, the body-centered cubic ferrite phase has a high hydrogen diffusion rate, making its hydrogen embrittlement sensitivity particularly prominent [7,8]. Therefore, how to effectively suppress the penetration and diffusion of hydrogen atoms into the pipeline steel is a key scientific issue that must be solved to ensure the long-term safe service of hydrogen pipelines.

Among the many hydrogen embrittlement protection strategies, coating hydrogen barrier coatings on metal surfaces is recognized as one of the most direct and effective methods. To address these issues, organic polymer-based composite coatings have attracted increasing attention from researchers in recent years. As a coating matrix, epoxy resin (EP) has become the most representative polymer coating material due to its excellent adhesion, good chemical corrosion resistance, low curing shrinkage rate, and flexible processing properties [9,10]. The abundant epoxy and hydroxyl groups on the molecular chain of epoxy resin can chemically react with amine curing agents and active sites on the metal substrate surface, forming highly crosslinked three-dimensional network structures and strong interfacial bonds [11]. However, pure epoxy resin coatings have limited barrier ability to hydrogen, mainly due to the large free volume between molecular chain segments, providing channels for hydrogen atom penetration [12].

To improve the hydrogen barrier performance of polymer coatings, researchers have widely adopted strategies in recent years by introducing two-dimensional nano-fillers. Among them, graphene stands out due to its unique structural and performance advantages. Both theoretical calculations and experimental studies show that a perfect graphene monolayer has extremely high gas impermeability: its six-membered ring hole geometric is only 0.064 nm, much smaller than the kinetic diameter of a hydrogen molecule (0.314 nm); at the same time, the dense electron cloud formed by π bonds exerts strong repulsion force on tunneling particles, with a theoretical barrier of hydrogen atoms penetrating the center of the graphene benzene ring reaching 4.61 eV, which is much greater than the adsorption energy of the C–H bond formed with graphene (0.18 eV) [13,14].

Based on these advantages, researchers initially mainly adopted a blending strategy of uniformly dispersing graphene in the coating matrix to prepare hydrogen-blocking coatings. Unlike blending strategies, multilayer sandwich structure coatings concentrate fillers at specific interface layers, alternating the construction of filler-enriched layers and polymer layers to form a multi-interface system. This structural design allows the interfaces between different material layers to scatter or reflect diffusing hydrogen atoms, with each additional interface equivalent to an additional barrier. Cai and others designed a composite sandwich structure coating composed of graphene-epoxy resin/silicon carbide epoxy resin/graphene-epoxy resin, utilizing the synergistic blocking effect of multiple interfaces to achieve hydrogen barrier performance significantly superior to single-layer coatings [15]. Wan et al. found that when preparing CGO/EP composite coatings, the CGO layers exhibit regular lateral arrangements, forming a dense laminar flow structure, and with a dosage of 0.25 wt%, hydrogen blocking efficiency can reach over 93% [16]. However, the hydrogen barrier performance of interlayer structures largely depends on interlayer bonding quality and reasonable matching of thicknesses between layers. Excessive layers not only increase the total coating thickness but also cause accumulation of residual internal stress, which may induce microcracks at interfaces, which instead become rapid diffusion channels for hydrogen atoms. Compared to blended composite coatings, interlayer structures are more complex, requiring layer-by-layer coating and curing, which is time-consuming. However, their advantage is that they avoid degradation of mechanical properties caused by a high

filler content. It is worth noting that most existing studies focus on interlayer structures with a low packing content (usually below 5 wt%), and there is still a lack of systematic comparative studies on the hydrogen-blocking behavior of interlayer structures under higher addition amounts or different layer counts.

To address these shortcomings, this study designs a series of graphene/epoxy composite coatings with different numbers of layers and prepares multilayer graphene interlayer structural coatings for comparison, systematically investigating the effects of packing content and interface structure on the hydrogen barrier performance, mechanical properties, and corrosion resistance of coatings. It is hoped that through this work, the intrinsic relationship between the number of epoxy resin layers and hydrogen barrier efficiency will be revealed, providing an experimental basis for material selection and structural design of protective coatings on the inner walls of hydrogen pipelines.

2. Experimental Materials and Methods

The X80 pipeline steel substrates were cut into dimensions of 50 mm × 50 mm × 1 mm. The chemical composition of the X80 pipeline steel (wt%) was as follows: C ≤ 0.12, Si ≤ 0.45, Mn ≤ 1.8, P ≤ 0.025, S ≤ 0.015, Nb ≤ 0.07, V ≤ 0.11. Prior to coating deposition, the substrate surfaces were mechanically ground with #60, #220, and #400 grit SiC abrasive papers. Grinding was intentionally terminated at #400 grit to retain a certain degree of surface roughness, thereby enhancing the mechanical interlocking and adhesion of the subsequent coating. After grinding, the specimens were ultrasonically cleaned in absolute ethanol for 3 min to remove residual grease and debris. Finally, the samples were dried in an oven and kept ready for the spray-coating process.

For this experiment, the slurry was pure epoxy slurry (EP). The EP was supplied by Baichang Coatings Co., Ltd., Changzhou, China: epoxy topcoat, curing agent, and thinner were mixed in a mass ratio of 4:1:1. Using an ME3002 electronic balance, 16 g of epoxy resin, 4 g of epoxy resin curing agent, and 4 g of epoxy resin thinner were measured, respectively. The mixture was placed in a 100 mL beaker, stirred at low speed with a glass rod until uniform, and left to degas for 15 min. The substrate surface was prepared by spray coating. The preparation process for the three multilayer coatings is as follows: EP + GC + EP-1 uses a layer-by-layer coating process, sequentially coating EP slurry, GC coating, and EP slurry. After each layer, the coating was leveled at room temperature for 15 min; the epoxy layer was cured at 70 °C for 1 h and air-cooled, while the graphene (by Suqian Nakaite New Materials Technology Co., Ltd.) layer was cured at 70 °C for 3 h and cooled in a furnace. The preparation process for EP + GC + EP-2 is similar, except that after coating the base layer EP, the base layer is precured at 70 °C for 30 min until it becomes semi-gel-like; then, cooling is followed by subsequent coating. For the EP + GC coating, the GC coating is first applied on the substrate, and after the surface is dry, the EP slurry is applied. Other process parameters are the same as the previous two. A light microscope and an FEI Nova Nano SEM450 scanning electron microscope (SEM) were used to observe the coating surface and cross-sectional morphology and to measure the actual thickness. Gold spraying is required before observing the coating surface.

The adhesion strength of single and composite coatings is measured quantitatively using the pull-open method, with specific operations following the national standard "GB/T 5210—2006 [17]: Pull-apart Adhesion Test for Colored and Varnished Paints." First, use 60#, 120#, and 400# sandpaper to sequentially sand the test surface and the opposite side to ensure both surfaces are clean and free of contaminants. Next, bond two coaxial test posts with a diameter of 15 mm to the test surface with adhesive, maintaining coaxial curing for 24 h. Finally, the specimen was placed on SAAS's EUT5105 universal testing machine and subjected to vertical tension at a constant vertical speed not exceeding 1 MPa/s, controlled

within 90 s [17], recording the maximum tensile force required for adhesion failure between the coating and substrate.

Hydrogen resistance testing was conducted with reference to the national standard "GB/T 30074-2013 [18]: Methods for Measuring Hydrogen Permeation (Absorption and Migration) in Metals Using Electrochemical Technology." A Devanathan-Stachurski dual-electrolyzer cell system was used, where the anode cell contained a sealed solution containing 0.1 mol/L NaOH, and the cathode cell contained a solution containing 0.1 mol/L NaOH and 0.3 g/L thiourea (Figure 1). The specimen was clamped between the two cells, with nickel pre-plated on the anode surface and coated specimens on the cathode surface, exposing an area of 3.14 cm^2 and a thickness of 1 mm. During testing, a 0.2 V constant potential was first applied to the anode side; after the background current stabilized, a 0.5 V constant potential was applied to the cathode side for electrolysis. The permeation current generated by oxidation on the anode side was recorded in real time by the electrochemical workstation, which generates a hydrogen permeation curve [8].

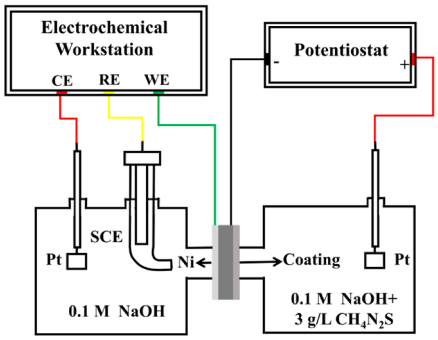


Figure 1. Diagram of the electrochemical hydrogen permeation device.

Potentiodynamic polarization tests were performed using an electrochemical workstation (Corrtest Instruments CS350 M, Wuhan, China) to evaluate the corrosion resistance of the coating after immersion in NaCl solution. The tests were conducted with an exposed area of 0.8 cm^2 and an electrolyte volume of 250 mL (at room temperature (25 °C)), and three parallel samples were prepared for each condition. The open-circuit potential (OCP) was measured before each test until a stable potential was reached, and all measurements were conducted under ambient air exposure (naturally aerated conditions). The working electrode was the coated specimen, with a saturated calomel electrode (SCE) used as the reference electrode and a platinum sheet electrode (Pt) used as the auxiliary electrode. The specimens were immersed in a 3.5 wt% NaCl solution. Polarization tests were performed by scanning from an initial potential of −1.5 V to a final potential of +1.5 V at a scan rate of 5 mV/s with a data sampling rate of 1 Hz.

The functional groups on the surfaces of the EP, modified graphene, and composite coatings were analyzed using X-ray photoelectron spectroscopy (XPS, Thermo ESCALAB 250XI, Thermo Fisher Scientific, Waltham, MA, USA). The acquired XPS data were processed and fitted using Avantage software, with all binding energies calibrated to the adventitious carbon C1s peak at 284.8 eV.

The three-dimensional surface morphology and areal surface roughness (Sa) of the coatings before and after hydrogen charging were characterized using a digital microscope (VHX-5000, Keyence, Japan). For each specimen, the 3D surface topography was captured over a scanning area of 1.0 mm × 1.0 mm at a magnification of 500×. To ensure statistical reliability, measurements were performed at three randomly selected locations on each sample. The Sa values were calculated automatically by the instrument's built-in analysis software according to the ISO 25178 standard.

3. Results and Discussion

The surface macroscopic morphologies of the prepared epoxy resin (EP), EP + graphene + EP-1 three-layer coating, EP + graphene + EP-2 three-layer coating, and graphene + EP double-layer coating are shown in Figure 2. The outermost layer of the four types of coatings is epoxy resin, with a very smooth surface that is uniform and dense overall, without obvious macroscopic cracks, protrusions, holes, or delamination.

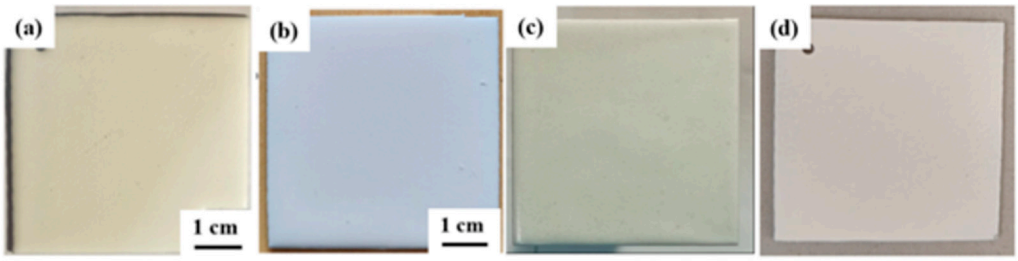


Figure 2. Coating surface morphologies of (**a**) EP, (**b**) EP + graphene + EP-1, (**c**) EP + graphene + EP-2, and (**d**) graphene + EP.

Figure 3 shows SEM images of the EP surface under different magnifications. Observed at low magnification (Figure 3a), the coating is overall continuous and uniform, with no obvious microcracks or pores detected, demonstrating good leveling and film-forming capability. At high magnification (Figure 3b), micron-level white particles are distributed on the dense resin matrix, representing TiO_2 white pigments and fillers.

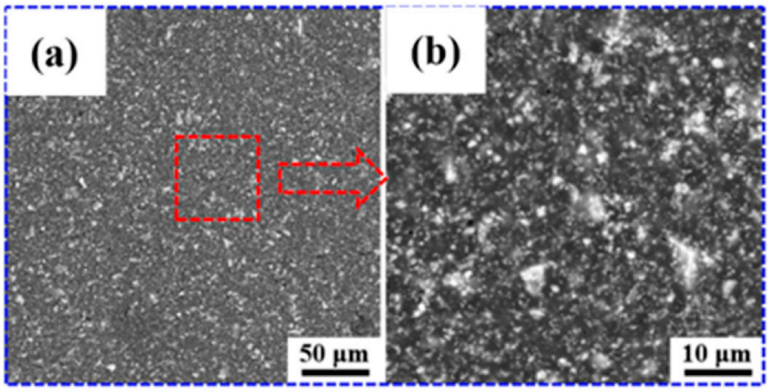


Figure 3. SEM micromorphology of the EP surface: (**b**) is a magnified view of the red boxed region in (**a**).

To clarify the thickness characteristics of different coatings, thickness tests were conducted on each coating system, and the results are shown in Figure 4. The single-layer EP coating is thinner at 201 μm. The thickness of the three-layer coatings, EP + graphene + EP-1 and EP + graphene + EP-2, is 370 μm and 290 μm, respectively, significantly thicker than the pure EP coating. In contrast, the thickness of the double-layer EP + graphene coating is reduced to 255 μm. This indicates that multilayer design can significantly increase the total coating thickness, with the gain mainly coming from the stacked EP layers, with a graphene single-layer thickness of about 20–50 μm.

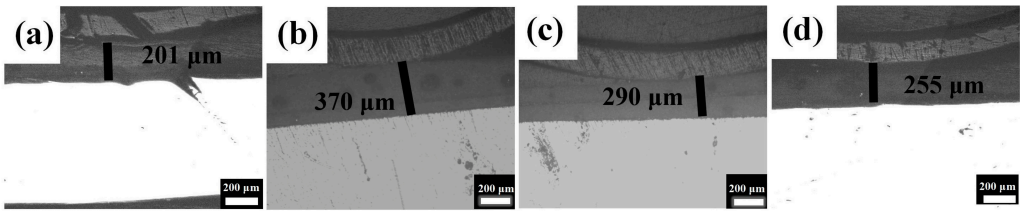


Figure 4. Coating cross-sectional thickness: (**a**) EP, (**b**) EP + graphene + EP-1, (**c**) EP + graphene + EP-2, and (**d**) graphene + EP.

The adhesion strength of the coating was tested using the drawing method. Figure 5 shows the morphology of the four coatings after drawing. Analysis of the pull-out surfaces shows that for single-layer EP coatings, the pull-out fracture did not expose the steel matrix, as shown in Figure 5a, indicating that due to the relatively thick coating, fractures occurred between coatings, resulting in cohesive failure. However, the substrate of three groups of samples (EP + graphene + EP-1, EP + graphene + EP-2, and EP + graphene) with three composite coatings (EP + graphene + EP-1, EP + graphene + EP-2, and EP + graphene) was not exposed, as shown in Figure 5b–d, with all exposing the graphene coating surface, indicating that the bottommost coating was not pulled off; fracture failure occurred inside the coating, which is a typical cohesive failure mode. Among them, the graphene surfaces at the fracture surfaces of the EP + graphene + EP-1 and EP + graphene + EP-2 coatings are relatively rough, indicating that the fracture occurs between graphene layers; whereas the fracture surfaces of the EP + graphene coating show bright graphene with residual epoxy resin, indicating that the fracture location is at the interface between the epoxy resin and graphene.

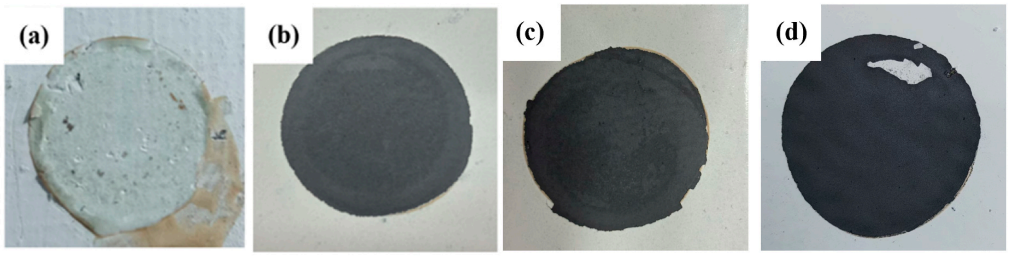


Figure 5. Coating tensile fracture morphology: (**a**) EP, (**b**) EP + graphene + EP-1, (**c**) EP + graphene + EP-2, and (**d**) graphene + EP.

Figure 6 shows the results of the bonding strength tests for different coatings. For pure EP coatings, the coating has the highest adhesion strength of 28.87 MPa. This cohesive failure behavior can be attributed to the strong interfacial bonding between the epoxy resin and the substrate: on one hand, after curing, the epoxy resin forms a three-dimensional crosslinking network that can embed itself on the substrate surface like a "hook," producing mechanical interlocking effects. On the other hand, polar groups such as hydroxyl and ether bonds in the crosslinking network can form hydrogen bonds with metal atoms on the substrate surface, further enhancing interfacial bonding. There are significant differences in adhesion strength among coatings with different layered structures, but overall, the double-layer coatings outperform the three-layer coatings. EP + GC + EP-1 and EP + GC + EP-2 have weaker bonding strength, at 10.16 MPa and 11.38 MPa, respectively. The EP + GC double-layer coating has a bonding strength of 19.6 MPa, demonstrating the highest bonding strength. This result indicates that the bonding strength between graphene and the matrix is stronger than that between epoxy resin and graphene. In the EP + graphene coatings, the graphene single-layer thickness is about 20–50 μm; therefore, the graphene sheets are

evenly dispersed, forming a continuous physical barrier and forming sufficient chemical bonds with the epoxy resin, thus achieving the highest bonding strength. However, when the coating structure expands into three layers, both sides of the graphene are adjacent to the epoxy resin, forming a "sandwich" configuration. Under this structure, during drawing, the load must be sequentially transferred through the outer EP layer to the middle graphene layer, and then to the interface between the lower EP layer and the matrix. Multiple interfaces extend the force transmission path and make stress more likely to concentrate inside the graphene layer, causing the coating to break inside and reducing its adhesion strength.

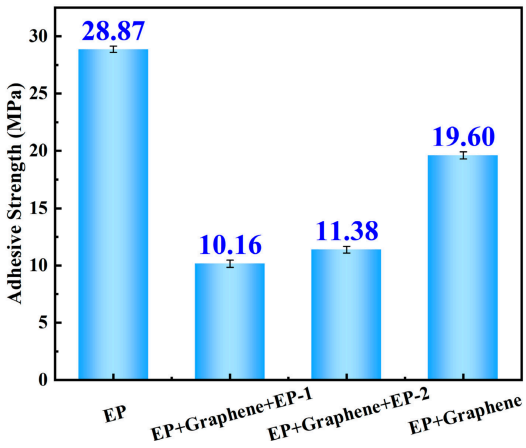


Figure 6. Coating adhesion strength.

To clarify the surface element composition and content distribution of the EP + graphene bilayer coating, X-ray photoelectron spectroscopy (XPS) was used to perform full-spectrum scanning analysis on the sample surface. From the full XPS spectrum (see Figure 7a), characteristic signals of five elements—C, O, N, Si, and Cl—were detected on the coating surface, with atomic percentages of C1s (66.2%), O1s (22.2%), N1s (3.7%), Si2p (6.7%), and Cl2p (1.1%), respectively. Among them, C has the highest peak intensity and is the dominant element on the coating surface, with sources including sp2 hybrid carbon in the graphene framework and the organic carbon chain structure in the epoxy resin matrix. O is the second major element, mainly derived from epoxy and hydroxyl functional groups in the epoxy resin, as well as residual oxygen-containing groups on the graphene surface and oxygen elements in silicon-containing components. It is an important component of the epoxy resin curing system and modification components. The characteristic peak of N corresponds to the amine curing agent component in the epoxy resin curing system, a functional element normally introduced during coating preparation, and its presence proves that the curing reaction of epoxy resin is effectively carried out. The Si signal originates from the added silane coupling agent in the coating system, which is typically used to improve the dispersion of graphene in the epoxy resin matrix and to enhance the interfacial adhesion between the coating and the X80 pipeline steel matrix. It is one of the key elements in composite coating modification design. No characteristic signal of Fe in the X80 pipeline steel matrix was detected in the full spectrum (the Fe2p characteristic peak is at the ~711 eV binding energy). These results show that the graphene/epoxy resin double-layer coating has excellent surface integrity in the test area, with the outer epoxy resin layer completely covering the internal graphene layer and the steel matrix, with no penetrating defects such as pinholes or cracks, providing a fundamental guarantee for the coating's corrosion resistance.

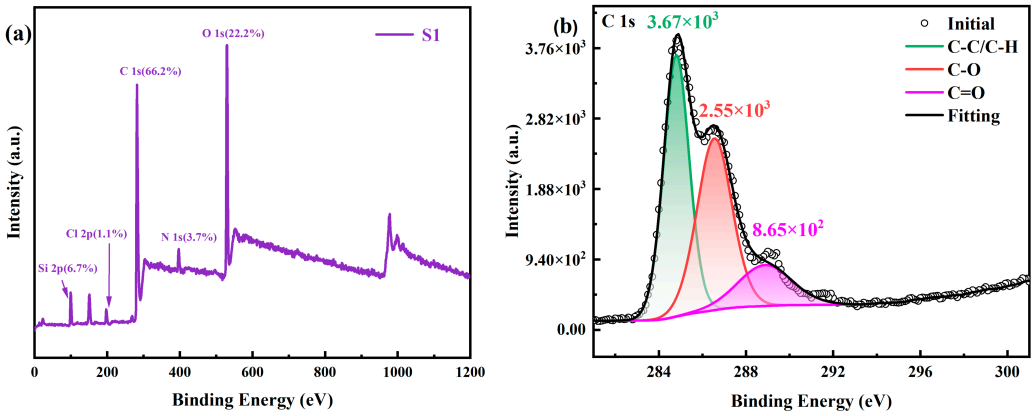


Figure 7. Full spectrum of XPS with graphene + EP dual-layer coating: the spectra include a wide scan survey (**a**), C 1s core-level (**b**).

To further clarify the chemical valence states and bonding forms of carbon on the surface of EP + GC coatings, high-resolution XPS peak fitting was performed on the characteristic peaks of C1s to analyze the C1s spectra of graphene and EP (see Figure 7b). According to different binding energies, the C1s spectra were fitted into three characteristic peaks: one at 284.8 eV, corresponding to the C–C/C–H bond; one at 286.2 eV, corresponding to the C–O bond; and the last peak is at 288.5 eV, corresponding to the C=O bond. The fit strength and proportion of each peak reflect the distribution characteristics of different carbon-based functional groups in the coating. Among them, the C1s signal is stronger and closer to the pure EP coating, indicating that its carbon framework structure dominates while still retaining characteristic peaks of O1s and Si2p. The peak shape of C1s is highly similar to EP, composed of three characteristic peaks: C–C/C–H, C–O, and C=O, with no obvious new chemical bond signals, indicating that after introducing silicon and carbon components, the coating still maintains a carbon chemical environment similar to epoxy resin [19]. However, compared to EP coatings, double-layer coatings have more C-O bonds, proving that EP and graphene layers are connected via C–O bonds. This further demonstrates that the better adhesion of layered coatings is due to bonding between coatings.

Using the Devanathan–Stachurski dual-electrolyzer device, hydrogen permeation tests were conducted on blank X80 steel substrates and graphene/epoxy resin composite coating samples of different structures. The hydrogen permeation current density variation curve over time is shown in Figure 8, with the complete curve reflecting the overall trend over a 40,000 s test cycle. The hydrogen permeability curve of the X80 steel matrix exhibits typical metallic hydrogen diffusion characteristics: after polarization current is applied on the cathode side, hydrogen atoms rapidly form and diffuse across the substrate surface, reaching a stable plateau state within about 2000 s, with a steady-state hydrogen permeation current density of about 2.8×10^{-5} A/cm^2. These results indicate that X80 steel without coating protection has almost no barrier to hydrogen atoms, allowing hydrogen atoms to rapidly diffuse through the matrix lattice. This is an important reason why pipeline steel is prone to hydrogen-induced cracking failure in hydrogen-containing corrosive environments.

The hydrogen permeation curve of the graphene + epoxy resin bilayer coating dropped rapidly at the initial stage of testing, entered a fluctuating upward phase after 10,000 s, and showed significant current density peaks near 22,500 s and 35,000 s. The final calculated steady-state hydrogen permeability current density was 3.37×10^{-6} A/cm^2. Compared with the matrix, the steady-state hydrogen permeation current density of the graphene + epoxy resin bilayer coating decreased by about 88%, demonstrating good hydrogen barrier performance. The steady-state hydrogen permeation current density of EP + graphene + EP-1 and EP30 min + graphene + EP-2 coating samples further decreased by 1.07×10^{-6} A/cm^2

and 1.08 × 10^{-6} A/cm^2, respectively, both lower than those of the double-coated samples, indicating that the hydrogen barrier performance of the three-layer coating structure is generally better than that of the double-layer structure. Among them, the current density curve of EP3 + graphene + EP-2 samples fluctuated less and remained more stable, indicating that the precuring process can improve interfacial compatibility of coatings, reduce microscopic defects, and further enhance coating density and hydrogen barrier stability.

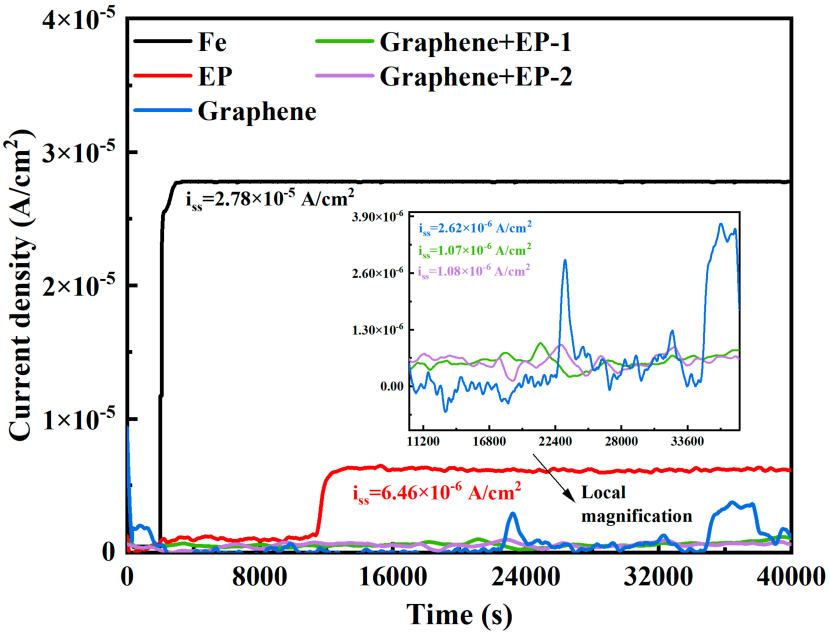


Figure 8. Hydrogen permeation curve of composite coatings.

The hydrogen barrier capacity of the coating was evaluated using the hydrogen diffusion coefficient D, hydrogen diffusion flux J, and hydrogen permeability reduction coefficient. The formula for the effective hydrogen diffusion coefficient D_{eff} is as follows [18,20]:

$$D_{eff} = \frac{L^2}{6t_{0.63}} \quad (1)$$

In the formula: D_{eff} is the effective hydrogen diffusion coefficient, cm^2/s;
L is the sample thickness, cm, with a sample thickness of 0.1 cm;
$t_{0.63}$ is the hydrogen permeation lag time, s.
Hydrogen diffusion flux: J_{ss} formula:

$$J_{ss} = \frac{i_{ss}}{FA} \quad (2)$$

In the formula: J_{ss} is the hydrogen diffusion flux, mol/(m^2·s);
i_{ss} is the hydrogen permeation current density, A/cm^2;
A is the sample exposure area, cm^2;
F is the Faraday coefficient, with a value of 96,485 C/mol.
The hydrogen permeability reduction factor (PRF) was used to evaluate the hydrogen permeability of materials [21].

$$PRF = \frac{J_{ss0}}{J_{ss1}} \quad (3)$$

In the formula, PRF is the hydrogen permeation reduction coefficient;
J_{ss0} is the steady-state hydrogen diffusion flux of the untreated substrate, mol/(m^2·s);
J_{ss1}, is the after coating treatment, and the steady-state hydrogen diffusion flux of the material is mol/(m^2·s).

According to Formula (1), the effective hydrogen diffusion coefficient is shown in Figure 9a; the effective hydrogen diffusion coefficient of the double-layer coating is 7.25×10^{-8} cm^2/s. The effective hydrogen diffusion coefficient of the two three-layer coatings is significantly lower than that of the two-layer coating. The EP + graphene + EP-1 coating has a hydrogen diffusion coefficient of 4.34×10^{-8} cm^2/s, which is about 40% lower than the double-layer coating 1%. The EP + graphene + EP-2 coating has a speed of 4.08×10^{-8} cm^2/s, which is the lowest among all samples. The three-layer structure design can significantly increase the diffusion resistance of hydrogen atoms within the system, effectively delaying the transport process of hydrogen atoms.

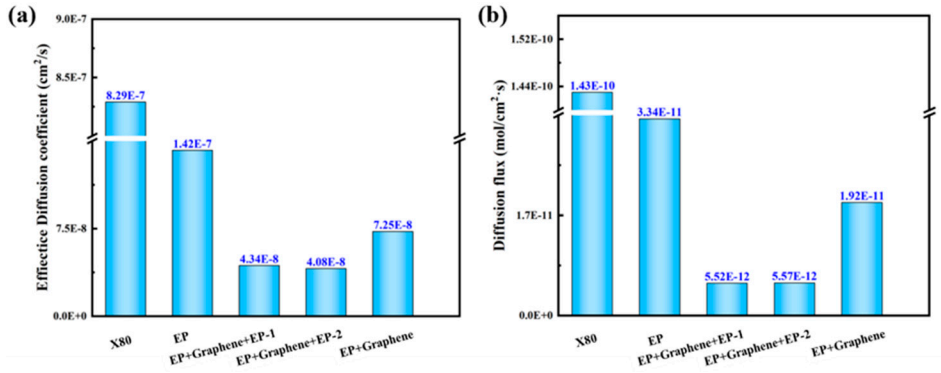


Figure 9. Coating hydrogen barrier properties: (**a**) effective hydrogen diffusion coefficient; (**b**) hydrogen diffusion flux.

Figure 9b shows the hydrogen diffusion flux calculated according to Formula (2). The results show that the variation pattern of hydrogen diffusion flux is consistent with the effective hydrogen diffusion coefficient, further verifying the difference in the effect of different coating thicknesses on hydrogen barrier performance. The hydrogen diffusion flux of the double-layer coating is 1.92×10^{-11} $mol/(cm^2 \cdot s)$. The hydrogen diffusion flux of the two three-layer coatings decreased by orders of magnitude: the EP + graphene + EP1 coating at 5.52×10^{-12} $mol/(cm^2 \cdot s)$ and the EP + graphene + EP2 coating at 5.57×10^{-12} $mol/(cm^2 \cdot s)$, which is consistent with the effective hydrogen diffusion coefficient. The PRF values, calculated according to Formula (3), are listed in Table 1 the larger the PRF value, the better the coating's hydrogen barrier performance. The calculation results show that graphene/epoxy composite coatings have a significant barrier effect on hydrogen penetration and diffusion. Compared to single-layer EP coatings (PRF = 5.84), multilayer coatings significantly improve hydrogen barrier performance. Among them, the three-layer coating has a PRF value exceeding 25, offering the best hydrogen barrier performance, and its hydrogen permeation current is correspondingly lower. The two-layer coating has a PRF value of only 11.43, indicating significantly weaker hydrogen barrier performance than the three-layer coating.

Table 1. Electrochemical parameters of hydrogen permeation.

Sample	i_{ss} ($\mu A \cdot cm^{-2}$)	T (s)
X80	27.8	2010
EP	6.46	11,731
EP + Graphene	3.73	22,981
EP + Graphene + EP-1	1.08	18,197
EP + Graphene + EP-2	1.07	9114

In summary, all graphene/epoxy resin composite coatings can significantly reduce the hydrogen permeation current density of the X80 steel matrix, effectively improving its hydrogen barrier performance. Different coating structures have significant differences in hydrogen barrier performance, with the three-layer coating structure demonstrating overall superiority to the two-layer structure. This is because the double-layer structure is thinner in total and has a relatively shorter diffusion path, which, to some extent, limits its hydrogen barrier capability. Among them, the topmost EP coating, with its interlaced molecular chains forming a high-density three-dimensional network, effectively extends the hydrogen atom diffusion path [22], while the lower graphene layer relies on its honeycomb carbon ring structure, making it almost impossible for hydrogen atoms to penetrate directly. The synergistic effect of the two forms a multi-layered physical barrier, significantly enhancing the overall hydrogen barrier performance of the composite coating. Therefore, for three-layer coatings, the more physical barriers there are, the longer the hydrogen diffusion path, and the better the hydrogen barrier performance.

Figure 10 shows the three-dimensional morphological changes in the coating surface before and after hydrogen charging, showing the EP + graphene double-layer coating (Figure 10a,a-1), EP + graphene + EP-1 (Figure 10b,b-1), and EP + graphene + EP-1 (Figure 10c,c-1). It can be seen that after hydrogen filling, the surface undulation of the double-layer coating is most pronounced, while the overall flatness is significantly reduced and localized spalling occurs. The change in surface roughness is also the greatest, increasing from 1.584 μm to 2.510 μm, indicating significant damage caused by hydrogen penetration; whereas the three-layer coating shows minimal changes in three-dimensional morphology and roughness before and after hydrogen filling, indicating that hydrogen penetration causes minimal damage to the coating surface.

Dynamic potential polarization technology was used to quantitatively evaluate the corrosion resistance of blank X80 pipeline steel and five types of graphene/epoxy resin composite coatings. The polarization curve was tested in 3.5 wt% NaCl solution at a scanning rate of 5 mV/s. The test results are shown in Figure 11. The dynamic potential polarization curve can be obtained by Tafel extrapolation by the Tafel method, yielding two core parameters: self-corrosion potential (E_{corr}) and self-corrosion current density (i_{corr}) [23], as shown in Table 2. The self-corrosion potential reflects the thermodynamic tendency of the material to undergo corrosion; the more positive the potential, the higher the thermodynamic stability. The self-corrosion current density reflects the kinetic rate of the corrosion reaction; the lower the current density, the lower the corrosion rate, and the better the corrosion resistance. Compared with the blank matrix, all graphene/epoxy resin composite coatings exhibited significant forward shifts in self-corrosion potential, and the self-corrosion current density decreased by orders of magnitude, indicating that the coatings can effectively suppress matrix corrosion reactions. Among them, the EP + graphene + EP-2 coating had the most positive self-corrosion potential at −0.37 V, with the lowest self-corrosion current density, while the EP + graphene double-layer coating had a higher current density and faster corrosion efficiency. Comprehensive dynamic potential polarization test results. The corrosion resistance performance of the four coatings ranked from best to worst as EP + graphene + EP-2 > EP + graphene + EP-1 > EP + graphene > EP. This is fully consistent with the electrochemical impedance spectrum and hydrogen permeation test results, further verifying the excellent protective performance of the three-layer structure coating and the significant improvement of corrosion resistance by the precuring process. The difference between the EP + graphene + EP-1 coating and EP + graphene + EP-2 coating lies in the curing method of the underlying EP coating, with the core differences being crosslinking density, hydrogen-blocking structure formation efficiency, and coating defect control.

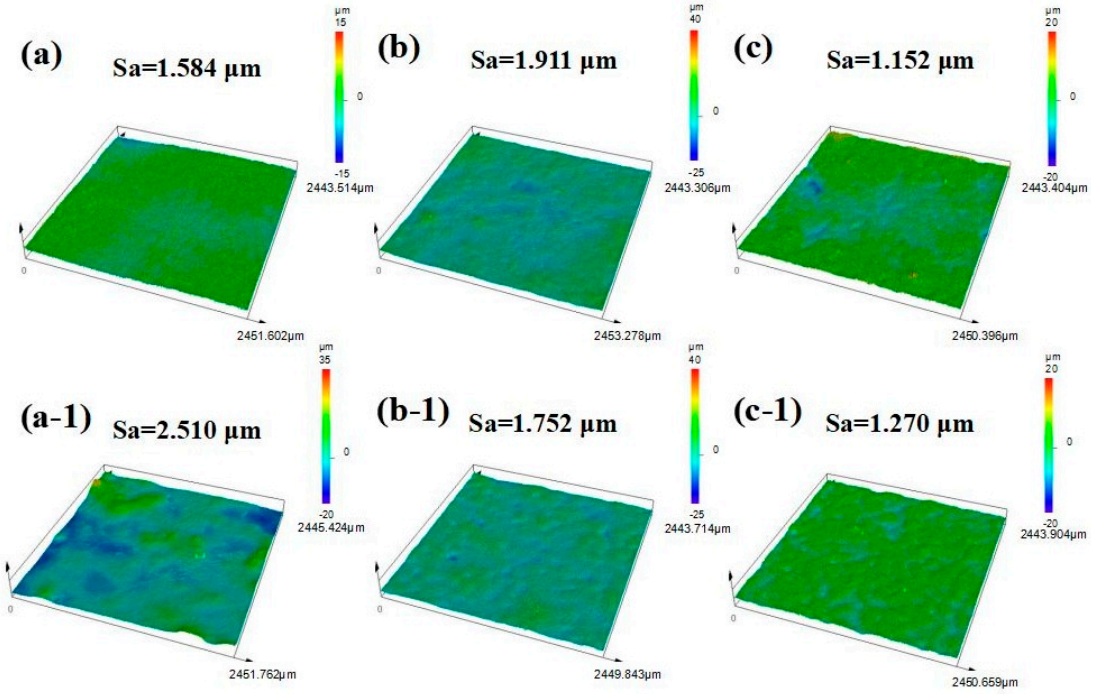


Figure 10. Three-dimensional ultra-depth micrographic pattern of the coating: (**a**,**a-1**) EP + graphene double-layer coating, (**b**,**b-1**) EP + graphene + EP-1, and (**c**,**c-2**) EP + graphene double-layer coating. (**a**–**c**) Unhydrogenated regions; (**a-1**,**b-1**,**c-1**) hydrogen-charged regions.

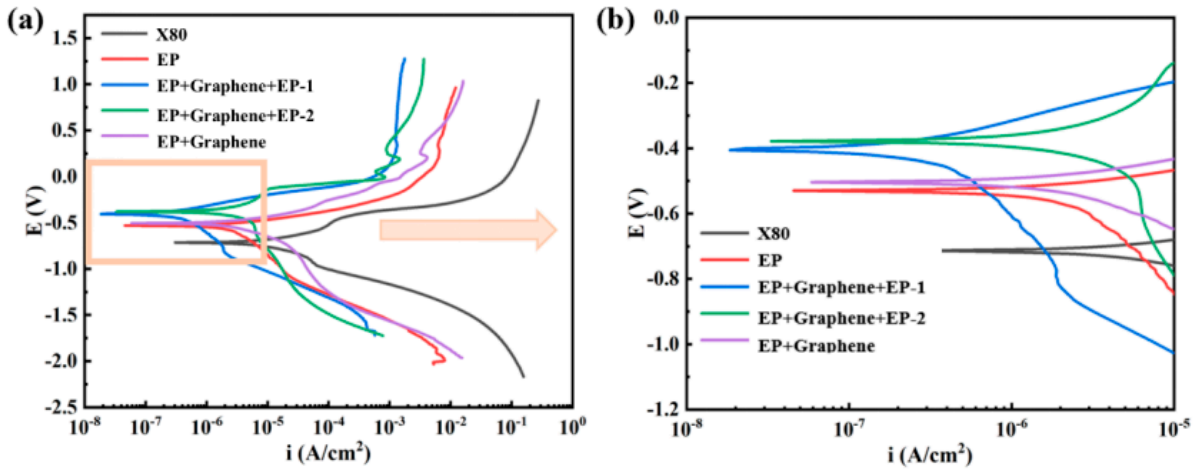


Figure 11. Polarization curves of different coating types: (**a**) Overall curve chart; (**b**) Local curve plot.

Table 2. Corrosion rate, corrosion current, and corrosion potential of each coating.

Coating Name	CR (mm/a)	i_{corr} (A/cm^2)	E_{corr} (V)
X80	0.177	1.511×10^{-5}	−0.714
EP	0.031	2.606×10^{-6}	−0.530
EP + Graphene + EP-1	0.006	5.189×10^{-7}	−0.403
EP + Graphene + EP-2	0.055	4.689×10^{-6}	−0.377
EP + Graphene	0.029	2.439×10^{-6}	−0.504

From the parameters obtained by Tafel extrapolation, the X80 substrate exhibited the poorest corrosion resistance. After applying the epoxy coating, the i_{corr} of EP decreased to 2.606×10^{-6} A/cm^2, the CR decreased to 0.031 mm/a, and the E_{corr} shifted positively to −0.530 V, indicating that the epoxy layer provides a pronounced barrier effect against

corrosive media. The EP + graphene bilayer coating showed an i_{corr} of 2.439×10^{-6} A/cm^2, a CR of 0.029 mm/a, and an E_{corr} of −0.504 V, which represents only a slight improvement over EP, indicating that simply introducing a graphene layer has a limited effect on improving the corrosion kinetics. In contrast, the three-layer EP + graphene + EP-1 coating exhibited the best overall corrosion resistance, with the lowest i_{corr} (5.189×10^{-7} A/cm^2), the lowest CR (0.006 mm/a), and an E_{corr} of −0.403 V. Compared with the X80 substrate, its i_{corr} and CR decreased by approximately 96.6%, and its E_{corr} shifted positively by 0.311 V. Compared with the EP coating, both i_{corr} and CR decreased by approximately 80%, and the E_{corr} shifted positively by 0.127 V. This indicates that the three-layer structure and the corresponding curing process can effectively suppress both the thermodynamic tendency and the kinetic rate of the corrosion reaction.

4. Conclusions

(1) Both graphene/epoxy resin composite coatings can significantly reduce the hydrogen permeation current density of the X80 steel matrix, with the three-layer sandwich structure (EP + GC + EP-1 and EP + GC + EP-2) having better hydrogen barrier performance than the double-layer structure (EP + GC). The effective hydrogen diffusion coefficients of the three-layer coating are 4.34×10^{-8} cm^2/s and 4.08×10^{-8} cm^2/s, respectively, about 40%–44% lower than the double-layer coating and about 95% lower than X80 bare steel. The three-layer structure significantly increases the diffusion resistance of hydrogen atoms by increasing the number of graphene/epoxy interfaces.

(2) The precuring process of the bottom epoxy further enhances the hydrogen barrier stability and density of the coating, resulting in minimal fluctuation in the hydrogen permeation curve of EP + GC + EP coatings and minimal roughness changes (surface roughness increased from 1.152 μm to 1.270 μm), indicating that precursor treatment can optimize interlayer interface bonding quality and reduce microscopic defects, making it an effective process method to improve hydrogen barrier performance in multilayer coatings.

(3) Coating structure has a significant impact on bonding strength. Double-layer coatings (EP + GC) have the highest bonding strength (19.6 MPa), while three-layer coatings have decreased bonding strength (10–11 MPa) due to the increased number of interface layers. However, all coatings fracture mode is cohesive failure, with no interface delamination, indicating good adhesion between epoxy resin and the matrix and between layers.

(4) Electrochemical tests show that the corrosion resistance of the three-layer coating structure is significantly superior to that of the two-layer and pure epoxy coatings. Among them, the EP + GC + EP-2 coating has the most positive self-corrosion potential (−0.37 V) and the lowest self-corrosion current density, which is highly consistent with the hydrogen barrier performance evaluation results, verifying the comprehensive advantages of the three-layer sandwich structure in both hydrogen resistance and corrosion protection. This study provides support for the application of graphene/epoxy multilayer coatings in the protection of hydrogen transmission pipelines. These coatings are facile to fabricate, low-cost, and exhibit favorable hydrogen-blocking performance and strong interfacial adhesion.

Author Contributions: Validation, Q.C.; Formal analysis, Q.C.; Investigation, J.D.; Resources, X.Z.; Data curation, H.P.; Writing—original draft, H.P. and J.D.; Writing—review and editing, X.Z. and K.Z.; Supervision, H.L. and P.L.; Funding acquisition, H.L. and K.Z. All authors have read and agreed to the published version of the manuscript.

Funding: This research gratefully acknowledges the support of the Science and Technology Plan Project of the State Administration for Market Regulation (No. 2025MK188).

Institutional Review Board Statement: Not applicable.

Informed Consent Statement: Not applicable.

Data Availability Statement: The data presented in this study are available on request from the corresponding authors.

Conflicts of Interest: The authors declare no conflicts of interest.

References

1. Wang, Y.; Guo, C.H.; Chen, X.J.; Jia, L.Q.; Guo, X.N.; Chen, R.S.; Zhang, M.S.; Chen, Z.Y.; Wang, H.D. Carbon peak and carbon neutrality in China: Goals, implementation path and prospects. *China Geol.* **2021**, *4*, 720–746. [CrossRef]
2. Yi, X.; Lu, T.; Li, Y.; Ai, Q.; Hao, R. Collaborative planning of multi-energy systems integrating complete hydrogen energy chain. *Renew. Sustain. Energy Rev.* **2025**, *210*, 115147. [CrossRef]
3. Wang, H.; Tong, Z.; Zhou, G.; Zhang, C.; Zhou, H.; Wang, Y.; Zheng, W. Research and demonstration on hydrogen compatibility of pipelines: A review of current status and challenges. *Int. J. Hydrogen Energy* **2022**, *47*, 28585–28604. [CrossRef]
4. Abe, J.O.; Popoola, A.P.I.; Ajenifuja, E.; Popoola, O.M. Hydrogen energy, economy and storage: Review and recommendation. *Int. J. Hydrogen Energy* **2019**, *44*, 15072–15086. [CrossRef]
5. Li, X.; Yin, J.; Zhang, J.; Wang, Y.; Song, X.; Zhang, Y.; Ren, X. Hydrogen embrittlement and failure mechanisms of multi-principal element alloys: A review. *J. Mater. Sci. Technol.* **2022**, *122*, 20–32. [CrossRef]
6. Meda, U.S.; Bhat, N.; Pandey, A.; Subramanya, K.; Raj, M.L.A. Challenges associated with hydrogen storage systems due to the hydrogen embrittlement of high strength steels. *Int. J. Hydrogen Energy* **2023**, *48*, 17894–17913. [CrossRef]
7. Askari, A.; Aliofkhazraei, M.; Afroukhteh, S. A comprehensive review on internal corrosion and cracking of oil and gas pipelines. *J. Nat. Gas Sci. Eng.* **2019**, *71*, 102971. [CrossRef]
8. Shi, K.J. In-Situ Preparation and Properties of Multilayer Graphene Hydrogen Barrier Coating on Pipeline Steel. Ph.D. Thesis, South China University of Technology, Guangzhou, China, 2021.
9. Yuan, S.; Zhang, S.; Wei, J.; Gao, Y.; Zhu, Y.; Wang, H. Materials selection, design, and regulation of polymer-based hydrogen barrier composite coatings, membranes and films for effective hydrogen storage and transportation: A comprehensive review. *Int. J. Hydrogen Energy* **2024**, *91*, 555–573. [CrossRef]
10. Wan, H.; Cheng, Z.; Song, D.; Chen, C. Preparation and performance study of waterborne epoxy resin/non-covalent modified graphene oxide hydrogen barrier coatings. *Int. J. Hydrogen Energy* **2024**, *53*, 218–228. [CrossRef]
11. Wan, H.; Min, W.; Song, D.; Chen, C. Research progress of hydrogen blocking coatings. *Mater. Chem. Phys.* **2024**, *328*, 130028. [CrossRef]
12. Joshi, M.; Adak, B.; Butola, B.S. Polyurethane nanocomposite based gas barrier films, membranes and coatings: A review on synthesis, characterization and potential applications. *Prog. Mater. Sci.* **2018**, *97*, 230–282. [CrossRef]
13. Nam, T.-H.; Lee, J.-H.; Choi, S.-R.; Yoo, J.-B.; Kim, J.-G. Graphene coating as a protective barrier against hydrogen embrittlement. *Int. J. Hydrogen Energy* **2014**, *39*, 11810–11817. [CrossRef]
14. Miao, M.; Nardelli, M.B.; Wang, Q.; Liu, Y. First principles study of the permeability of graphene to hydrogen atoms. *Phys. Chem. Chem. Phys.* **2013**, *15*, 16132–16137. [CrossRef] [PubMed]
15. Cai, K.; Jiang, B. Preparation and Characterization of Composite Hydrogen Barrier Coatings with (Graphene–Epoxy Resin)/(Silicon Carbide–Epoxy Resin)/(Graphene–Epoxy Resin) Sandwich Structures. *Coatings* **2025**, *15*, 518. [CrossRef]
16. Wan, H.; Min, W.; Bian, K.; Li, Y.; Yu, Z.; Chen, C. The design and performance study of MXene composite hydrogen barrier coatings. *Int. J. Hydrogen Energy* **2026**, *215*, 153893. [CrossRef]
17. *GB/T 5210-2006*; Paints and Varnishes—Pull-Off Test for Adhesion. China Standards Press: Beijing, China, 2006.
18. *GB/T 30074-2013*; Method of Measurement of Hydrogen Permeation and Determination of Hydrogen Uptake and Transport in Metals by an Electrochemical Technique. China Standards Press: Beijing, China, 2013.
19. Dashan, A.; Montazeri, S.; Haddadi, A.S.; Ramezanzadeh, B.; Qiang, Y.; Mekonnen, T.H. Dual-functional smart anti-corrosion coating based on Ti3C2Tx-MXene/Zr-UIO-66-NH2 reinforced epoxy. *Prog. Org. Coat.* **2025**, *206*, 109338. [CrossRef]
20. Lu, Y.; Liang, X.; Yang, H.; Fan, F.; Wang, Y.; Wang, L. Measurement and Application of Hydrogen Diffusion Coefficient of 0Cr16Ni5Mo Steel. *Dev. Appl. Mater.* **2025**, *in press*. [CrossRef]
21. Gao, C.; Chen, H.; Xu, H.; Wu, Z.; Dong, X. Molecular Dynamics Simulation of Hydrogen Permeation Behavior in Epoxy Resin Systems. *Polymers* **2025**, *17*, 1755. [CrossRef] [PubMed]

22. Tran, A.N.; Jang, S.; Joo, S. Graphene epoxy spray on 3D-printed acrylonitrile butadiene styrene substrates as O_2 gas barrier. *Appl. Surf. Sci.* **2019**, *497*, 143745. [CrossRef]
23. Kear, G.; Barker, B.; Walsh, F. Electrochemical corrosion of unalloyed copper in chloride media—-A critical review. *Corros. Sci.* **2004**, *46*, 109–135. [CrossRef]

Disclaimer/Publisher's Note: The statements, opinions and data contained in all publications are solely those of the individual author(s) and contributor(s) and not of MDPI and/or the editor(s). MDPI and/or the editor(s) disclaim responsibility for any injury to people or property resulting from any ideas, methods, instructions or products referred to in the content.